

Displacement and curvature estimation for the design of reinforced concrete slender walls

Leonardo M. Massone* and Jorge I. Alfaro

Department of Civil Engineering, University of Chile, Santiago, Chile

SUMMARY

Previous earthquakes, such as the 2010 Maule earthquake in Chile, have demonstrated the need to establish suitable predictors of compressive or tensile strains in concrete or steel in reinforced concrete shear walls, which can provide limit states or confinement requirements. Slender walls are commonly controlled by flexural deformations that can be divided into elastic and inelastic components. This study provides calibrated expressions for the elastic and inelastic components of flexural deformations using a fiber model for slender walls. These expressions are obtained for rectangular and T-shaped walls. The elastic component is dependent on the axial load and the boundary steel reinforcement ratio. The impact of wall coupling is investigated, which requires a correction for the elastic component. The investigation of the inelastic component is based on a plastic hinge model, in which the length of the plastic hinge is a function of the lateral inelastic drift of the wall among other parameters. The traditional linear inelastic curvature distribution over the wall height is also modified for cases with steel reinforcement with a long yield plateau or low strain hardening, which results in a larger curvature at the wall base. The distribution is validated with experimental data from the literature. Copyright © 2016 John Wiley & Sons, Ltd.

Received 09 July 2015; Revised 19 February 2016; Accepted 29 February 2016

KEY WORDS: slender wall; displacement; reinforced concrete; flexure; plastic hinge; fiber model

1. INTRODUCTION

The Mw8.8 magnitude earthquake of 2010 tested the design standard that is used in Chile for reinforced concrete buildings. An assessment of the condition of the buildings after the earthquake revealed damage to slender walls with rectangular and T-shaped cross-sections that were subjected to compression and lateral loads. The damage recurrently showed concrete cover spalling along a horizontal line in the wall web, buckling of longitudinal bars and fracturing of rebar in some cases (Fig. 1). These types of failures were caused by large strains in the most compressed areas of the walls, which were most likely preceded by critical tensile strains. All combined with a deficient detailing of boundary elements. This did not provide adequate concrete confinement or restraint of the buckling of the longitudinal bars (Wallace *et al.*, 2012; Massone *et al.*, 2012).

After the earthquake, observed deficiencies in the wall design prompted a modification of the Chilean standard of reinforced concrete design, which focused on the detailing requirements for the adequate performance of walls. The main changes are related to the incorporation of confinement requirements and damage limitations for walls (indirect limitation of axial load) by prescribing a maximum compressive deformation (Massone, 2013). Confinement is incorporated in the boundary elements of walls when the most compressed fiber exceeds a compression strain of 0.003, as required by the ACI 318-08 (2008) for the building design displacement δ_u . Strains in the most compressed fiber of concrete must not exceed 0.008. This requirement is determined for an ultimate curvature

*Correspondence to: Leonardo M. Massone, Department of Civil Engineering, University of Chile, Blanco Encalada 2002, Santiago, Chile.
E-mail: lmassone@ing.uchile.cl



Figure 1. Damage to building walls in Chile.

estimated with Eq. (1), where c is the depth of the neutral axis, h_w is the height of the wall, l_w is the length of the wall, δ_y is the yield displacement, ϕ_y is the yield curvature of the wall and l_p is the plastic hinge length (Fig. 2(a)). Fig. 2(a) shows the scheme of curvature distribution that is consistent with Eq. (1). The actual distribution of curvature usually exhibits a gradual increment within the plastic hinge zone. Eq. (1) can be simplified by concentrating all deformation (curvature) within a hinge at the wall base (Fig. 2(b)).

$$\phi_u = \phi_y + \frac{(\delta_u - \delta_y)}{l_p \left(h_w - \frac{l_p}{2} \right)} = \frac{\epsilon_c}{c} \leq \frac{0.008}{c} \quad (1)$$

To use Eq. (1), the following parameters need to be determined: the plastic hinge length, the yield curvature and the yield roof displacement. Paulay (2001, 2002) examined the elastic response of reinforced concrete walls and proposed estimating the yield curvature for walls as $\phi_y = \eta \frac{\epsilon_y}{l_w}$, where the coefficient η incorporates the effect of a bilinear moment-curvature diagram. A distribution of longitudinal reinforcement within the wall cross-section (boundary and web reinforcement) results in an initiation of yielding for the most extreme bar in tension, which reduces the stiffness of the moment-curvature diagram. The increments of curvature cause other bars to yield, which results in a gradual loss of stiffness until nominal or maximum capacity is attained. Extending the first yield to an equivalent yield for a bilinear moment-curvature diagram requires the amplification given by η . For rectangular walls with boundary elements and assuming a bilinear approximation of the

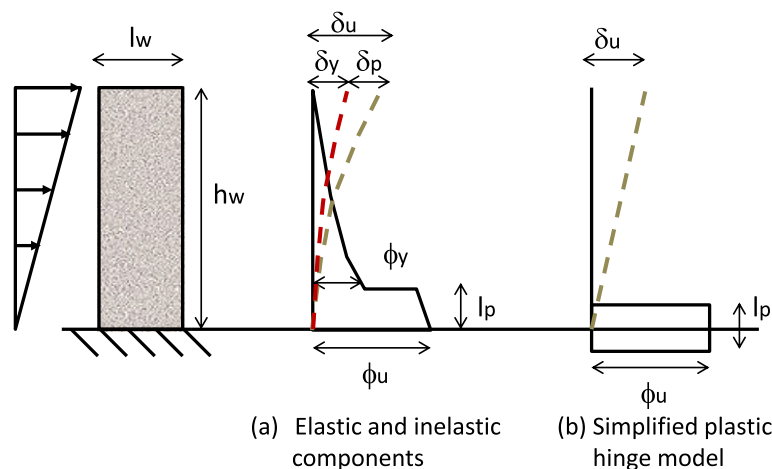


Figure 2. Plastic hinge model of wall—(a) elastic and inelastic components and (b) simplified plastic hinge model.

moment-curvature diagram, Paulay proposed $\eta = 1.8$. Thus, consideration of the first yield instead of the bilinear approximation may produce lower values. Considering that the majority of the walls in Chile did not incorporate confinement, performed adequately and primarily responded within the linear range, estimating the elastic component with the first yield is conservative. To complete the determination of the yield lateral roof displacement, Paulay modeled the seismic demand as a triangular distributed load over the height, which resulted in $\delta_y = \frac{11}{40} \phi_y h_w^2$. This expression considers a cracked cross-section over the full height, which results in larger displacement than expected for flexure.

In addition to the elastic contribution, which is distributed along the entire wall for the inelastic range, Eq. (1) assumes the existence of a plastic hinge in which all inelastic deformations are concentrated. The study by Paulay and Uzumeri (1975) estimates the length of the plastic hinge, which incorporates geometric aspects such as the wall length and the wall height. Bohl and Adebar (2011) include the contribution of the axial load for the majority of cases for a 2% top lateral drift that decreases with increased levels of axial load. Considering that the length of the plastic hinge increases with an increase in lateral roof displacement with a stable boundary element in compression, estimation of the plastic hinge length determined for moderate roof displacements might not be conservative.

Correct estimates of yield displacement and inelastic displacement by means of a plastic hinge model are relevant in modern design of buildings (Kang and Kim, 2014; Eslami and Ronagh, 2014), commonly through wall boundary detailing. Thus, this study calibrates expressions derived from a fiber model to estimate elastic and inelastic displacement components, which are based on variables, such as ϕ_y , δ_y , and l_p , to obtain the ultimate curvature (ϕ_u) expected in walls using a plastic hinge model. A distributed nonlinear plasticity model implemented in OpenSees (2000), which consists of fibers, is employed. The analytical expressions for the elastic part consider several variables (such as axial load, wall length, reinforcement ratio in the boundary elements and levels of coupling), which required a series of analyses. The investigation of the nonlinear response of the structure focuses on determining the variables that influence the plastic hinge length and the curvature distribution, which consists of the moment-shear ratio at the base, the wall length, the inelastic displacement attained by the wall, the strain hardening of the boundary reinforcement, the boundary reinforcement ratio and the level of axial load. These findings provide valuable information regarding how the plastic hinge grows with inelastic displacement and how the curvature concentrates within a region depending on steel properties and quantities, which is validated with tests results from the literature. Based on the monotonic response, the model is capable of predicting the behavior of walls in a zone that does not degrade, in which repetitive cycles do not increase strains or curvature. Limit states, such as the cyclic response of reinforcing bars, which are susceptible to buckling, can be captured with this approach by examining the maximum tensile and compressive strains in bars that usually initiate instability.

2. MODEL DESCRIPTION

In this section, the implementation of a nonlinear numerical model for slender walls composed of fibers, which are subjected to a pushover analysis, is described. The numerical fiber model implemented in OpenSees (2000) is a discretization of elements with cross-sections that consist of uniaxial fibers; each element exhibits the mechanical properties of concrete and steel. The model only considers the deformations produced by the axial and bending actions using the Bernoulli hypothesis. Discretized elements by the fiber model are characterized by axial deformation and curvature at the section level, which are associated with three degrees of freedom per node for a two-dimensional model: axial displacement, transverse displacement and rotation. The selected elements are based on the flexibility formulation such that equilibrium is guaranteed by the force interpolation functions (Spacone *et al.*, 1996), where two integration points located at the ends of the elements were considered. The model considered 20 elements (all of the same size—Fig. 3(a)) for the elastic analysis and 26 elements for the inelastic analysis. The additional elements in the inelastic case were placed at the base of the element by sub-dividing the last two elements in the elastic case to better distribute inelastic deformation at the plastic hinge location (Fig. 3(b)). The discretization of the cross-section in the elastic analysis considered eight fibers of concrete and steel in the web of the walls. Each boundary element ($0.1l_w$)

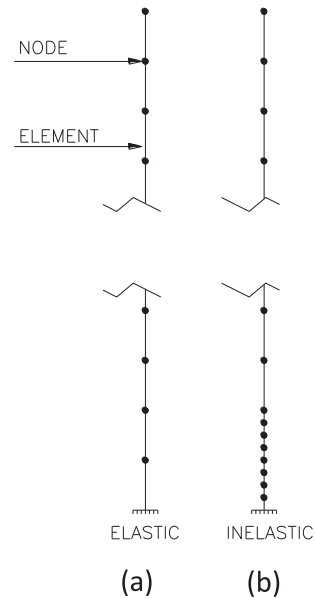


Figure 3. Wall longitudinal discretization—(a) elastic model and (b) inelastic model.

considered two fibers, which were doubled for the inelastic case (Fig. 4(a)), and incorporated fibers to represent the concrete cover. In the case of T-shaped walls, a similar discretization as for rectangular walls was selected for the web (Fig. 4(b)). The flange considered discretization in a direction opposite to the curvature axis just to differentiate sections of concrete and reinforcement. The model validation for the yield component and inelastic curvature distribution over the wall height is discussed in a related study (Alfaro, 2013). Here, the model comparison focuses on a test program that considers test variables, such as axial load, and steel material quantities and properties, which have an important impact on maximum curvature.

2.1. Steel reinforcement

For steel reinforcement, a tri-linear model was employed. For a monotonic loading state, this model requires four parameters: yield stress f_y , elastic stiffness E_s , post-yield stiffness (hardening) E_p and strain ε_{sh} at the beginning of hardening. For tensile steel, an apparent yield was considered, which is less than the value of the yield stress/strain of a bare steel bar, because the model works with average strains in the steel along the element. This situation considers the tension stiffening effect in concrete, which assumes the existence of areas in cracked zones in which concrete is not cracked and increases its post-cracking tensile stress and reduces the tensile stress in the steel bars (Belarbi and Hsu, 1994).

2.2. Concrete

The model considers concrete in tension with a linear behavior until cracking, followed by a decay that considers average stresses in concrete and steel based on the study by Belarbi and Hsu (1994) (tension stiffening). The compression behavior of concrete is determined by the Thorenfeldt equation, which is based on the Popovics curve (Popovics, 1973). The confinement effect provided by the stirrups is incorporated with the model by Saatcioglu and Razvi (1992).

3. ELASTIC CURVATURE AND DISPLACEMENT OF WALLS

A parametric analysis using a fiber model is used to calibrate expressions to estimate the yield curvature and the top lateral yield displacement of isolated walls. These analyses are performed for walls with rectangular and T-shaped cross-sections, in which the flange and the web are subjected to

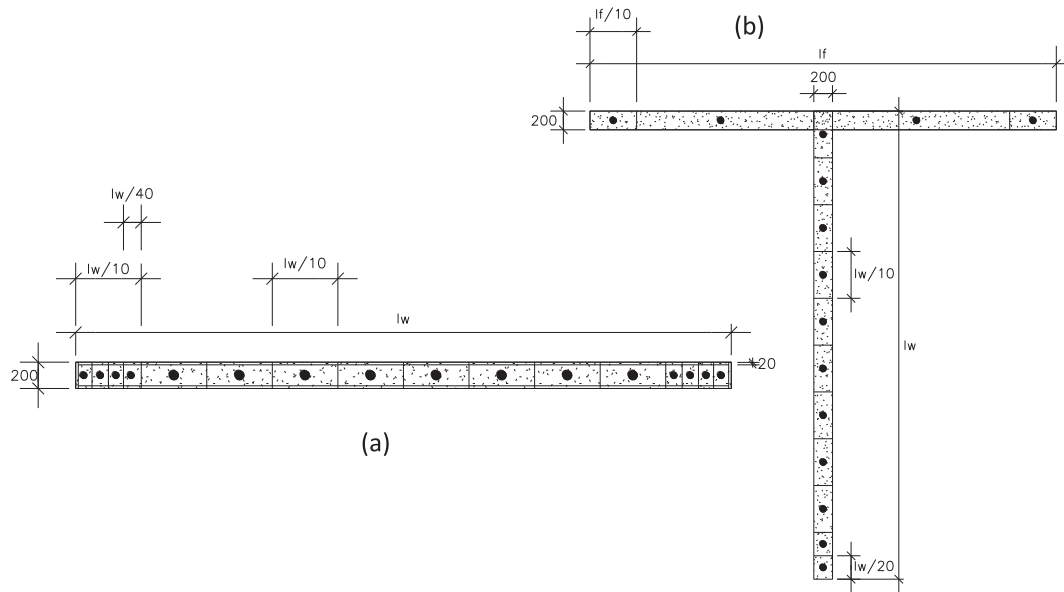


Figure 4. Wall section discretization—(a) rectangular and (b) T-shaped.

compression in the T-shaped cross-section. The main variables considered in the analysis are the axial load and the amount of reinforcement in the boundary elements, whereas the web reinforcement ratio is fixed as 0.25%. The model is subjected to a triangular load pattern and has a constant height. A building of 20 floors was considered with a story height of 2.7 m, with typical material properties for concrete and steel (concrete strength is $f'_c = 25$ MPa, and the steel yield strength is $f_y = 420$ MPa).

The two main parameters required for the analysis are the yield curvature (ϕ_y) and the yield displacement (δ_y). In both cases, the first yield is used. The typical pre-yield shear deformation in slender walls is small (Massone and Wallace, 2004). Using Eq. (2), the first yield top displacement (δ_y) can be calculated for a triangular lateral load pattern from a model that assumes a variable stiffness to the top of the structure (Fig. 2).

$$\delta_y = \alpha \phi_y h_w^2 \quad (2)$$

The yield curvature can be calculated with Eq. (3) and deduced from Fig. 5.

$$\phi_y = \frac{\epsilon_y}{\xi l_w} = K \frac{\epsilon_y}{l_w} \quad (3)$$

The section geometry, the distribution of cracking over the height, the level of axial load, the boundary reinforcement and other considerations affect the yield curvature and the yield displacement, which are reflected in coefficients α and K (Eqs. (2) and (3)), and are investigated in the following sections.

3.1. Parametric analysis—rectangular wall

The axial load is applied at the center of the cross-section. The wall width considered for all models is 0.2 m. In the analysis, the variables are defined as follows: wall length of 2.5 m, 5 m and 7.5 m are considered; axial load of $0.1f'_c A_g$, $0.2f'_c A_g$ and $0.3f'_c A_g$ are included; and regarding the boundary reinforcement ratio (over the boundary cross-section), a broad range of values is considered, although values between 5% and 6% are more frequently observed in buildings in Chile (Estay, 2008).

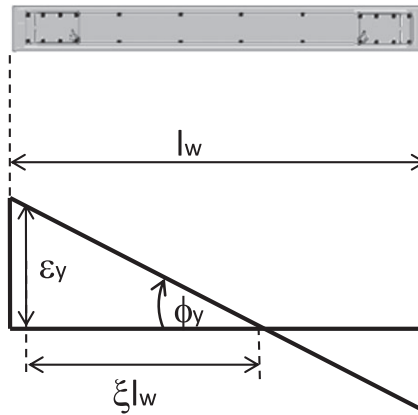


Figure 5. Yield curvature in wall cross-section.

In this analysis, the variables with the greatest impact on the yield curvature are the axial load and the amount of boundary reinforcement. The factor K can be parameterized in terms of these two variables, as shown in Eq. (4).

$$K = 1.25 + 1.69 \frac{P}{f'_c A_g} + 0.65 \rho_b \tag{4}$$

Values obtained from the numerical analysis are compared with the K values obtained with Eq. (4) in Fig. 6(a). Based on the results, a conservative value of $K=1.4$ can be considered for a boundary reinforcement ratio over 5% and axial loads over $0.1f'_c A_g$.

The variable α is dependent on the amount of boundary reinforcement. The α -values were calculated by considering the K values obtained with Eq. (4), which resulted in Eq. (5), as described in Fig. 6(b). According to Fig. 6(b), $\alpha=0.22$ is a conservative value for walls with a boundary reinforcement ratio larger than 5%.

$$\alpha = 0.33 \rho_b^{0.14} \tag{5}$$

3.2. Parametric analysis—T-shaped wall

The damage to buildings by the 2010 earthquake in Chile was concentrated on the first and ground floors. Structural configurations frequently consider central aisles that are formed by longitudinal walls, which are connected by transverse walls to form T-shaped walls (Massone *et al.*, 2012). Damage

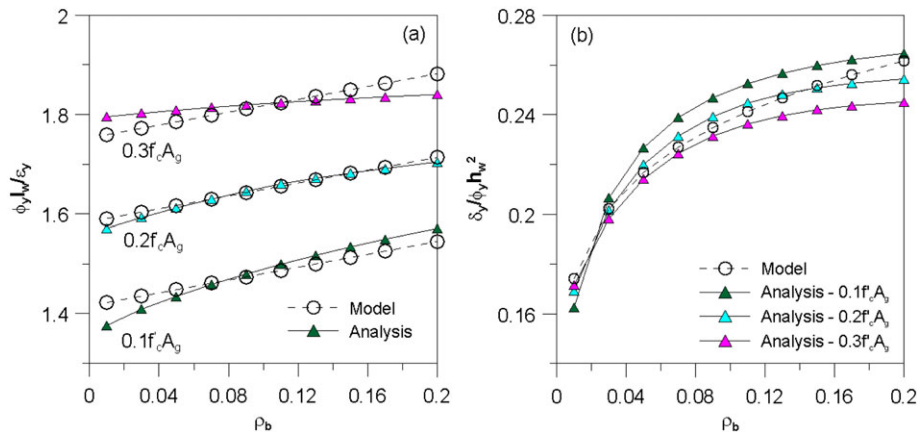


Figure 6. Isolated rectangular wall: (a) variation in K and (b) variation in α .

was particularly observed at the web end of T-shaped walls, where large compression strains occurred. This situation caused a loss of concrete cover, which combined with tension-compression cycles caused by seismic actions accelerates the buckling problems in longitudinal reinforcement and results in capacity degradation.

A T-shaped cross-section is defined by considering common arrangements observed in Chilean construction. The main longitudinal reinforcement was located in three areas: both flange ends and the web end. Distributed reinforcement was placed in the flange and the web of the wall. The thickness in the flange and the wall web is 20 cm, and the length of the flange is 5 m. Similar properties as for rectangular walls are considered here. The axial load was applied in the middle of the wall web. Three cases were considered: case 1 considers the same amount of total boundary reinforcement in the flange and the web end without distributed reinforcement in the flange; case 2 considers the same amount of total boundary reinforcement in the flange and the web end with distributed reinforcement in the flange (0.25%); and case 3 doubles the total amount of boundary reinforcement in the flange compared with the web end with distributed reinforcement in the flange (0.25%). The analysis was performed with the flange or the web end in compression to represent the direction of the seismic action.

3.2.1. Web in compression

The numerical analysis shows that the K value is dependent, as in the case of rectangular walls, on the level of axial load and the amount of boundary reinforcement of the web end, as shown in Eq. (6).

$$K = 1.32 + 1.67 \frac{P}{f'_c A_g} + 0.54 \rho_b \quad (6)$$

Fig. 7(a) shows the comparison between the values obtained with Eq. (6) and the values directly obtained from the analysis. The values obtained from the analysis for case 3 are not plotted because the wall begins to degrade in compression (web) prior to reaching the tensile yield strain (flange) for most of the analyzed cases. Similar to the rectangular wall cases, a value of $K=1.4$ is conservative.

The values of α were calculated considering the analytical expression of K (Eq. (6)). The coefficient α in the calculation does not consider the initial lateral displacement due to pure axial load (eccentricity). The results indicate that the parameter α is dependent on the amount of boundary reinforcement on the web end, as shown in Eq. (7). According to Fig. 7(b), $\alpha=0.22$ is a conservative value for walls with a boundary reinforcement ratio above 10%.

$$\alpha = 0.315 \rho_b^{0.15} \quad (7)$$

3.2.2. Flange in compression

The expression for K is dependent on the level of axial load and the amount of boundary reinforcement on the web end (Eq. (8)). In Fig. 8(a), the analysis results are compared with the model.

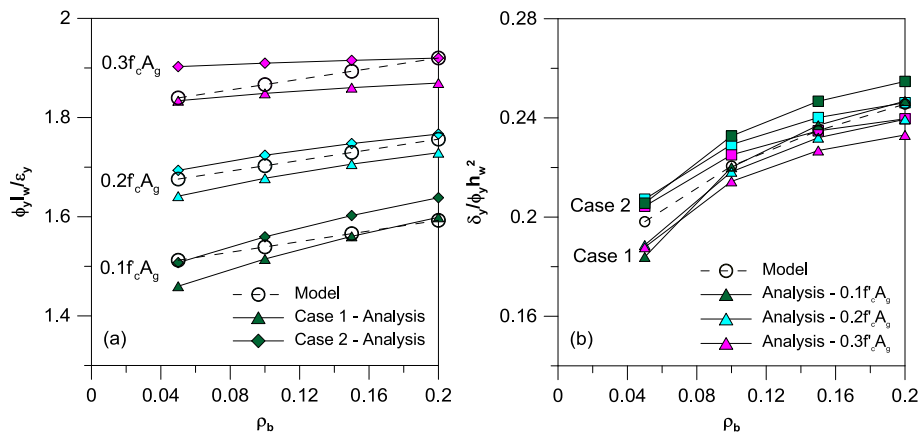


Figure 7. Isolated T-shaped wall with web in compression: (a) variation in K and (b) variation in α .

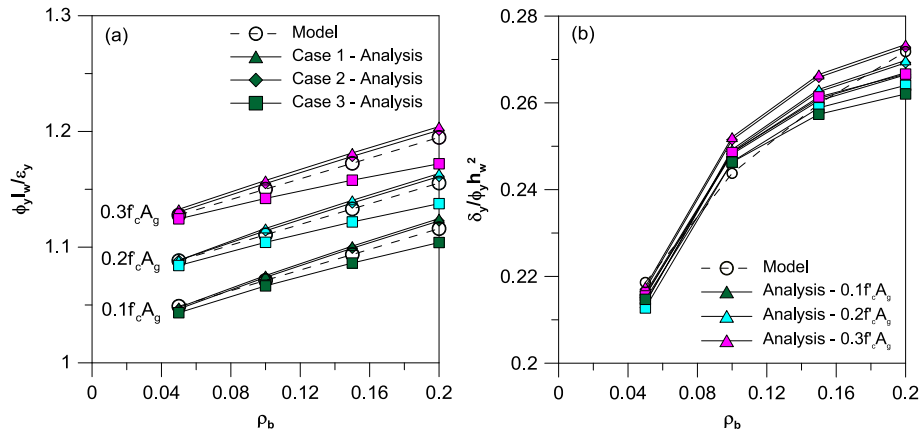


Figure 8. Isolated T-shaped wall with flange in compression: (a) variation in K and (b) variation in α .

$$K = 1.0 + 0.4 \frac{P}{f'_c A_g} + 0.45 \rho_b \quad (8)$$

The α values are consistent with Eq. (8) and determined according to Eq. (9), which are shown in Fig. 8(b).

$$\alpha = 0.35 \rho_b^{0.16} \quad (9)$$

Previous expressions are valid for an aspect ratio between the web and the flange length of 1.0. To consider the impact of the aspect ratio between the web and the flange length, an analysis was performed by varying the amount of boundary reinforcement, the axial load and the lengths of the flanges of the T-shaped walls (l_f between 2 and 8 m); the length of the wall web is 5 m ($l_w = 5$ m). Eq. (10) for T-shaped walls shows the dependency of the selected parameters on K . Fig. 8(a) shows the comparison for the equation using $l_f = 2$ m and $l_f = 8$ m for $P = 0.1 f'_c A_g$. The parameter can be assumed as $K = 1.0$ for T-shaped walls with a compression flange.

$$K = 0.86 + 0.46 \frac{P}{f'_c A_g} + 0.47 \rho_b + 0.11 \frac{l_w}{l_f} \quad (10)$$

The analysis of the α value (similar considerations as the previous cases) is demonstrated by Eq. (11). Fig. 8(b) shows the comparison for the equation using $l_f = 2$ m and $l_f = 8$ m. As in the previous cases, $\alpha = 0.22$ is considered to be conservative.

$$\alpha = 0.34 \rho_b^{0.15} + 0.01 \frac{l_w}{l_f} \quad (11)$$

4. YIELD CURVATURE AND DISPLACEMENT IN COUPLED WALLS

In Chile, the design of reinforced concrete buildings evolved after the earthquake in 1985. A significant change from old reinforced concrete wall buildings comprised the elimination of lintels as coupling elements between the walls located in hall areas. The slabs served their original roles. Contemporary buildings have long corridors; therefore, the main coupling given by the slab is installed between two walls located on the sides of the halls. In this section, the impact of coupling in the elastic response of rectangular walls is investigated.

4.1. Parametric analysis of coupled walls

For coupled walls, the model consists of two aligned rectangular walls connected by rectangular slabs at each level (floor); the slabs provide coupling to the system. The slabs are modeled as beam elements with hinges, in which plasticity is concentrated at their ends and steel fibers that model the positive and negative reinforcement in the slabs are incorporated.

A preliminary analysis considered dimensions and properties that are consistent with realistic building construction in Chile: axial loads of approximately $0.2 f_c A_g$, walls with a length of 5 m and a width of 20 cm, a boundary reinforcement ratio of 5% and slabs with a positive and negative reinforcement ratio of 0.2%, a thickness of 15 cm, an effective width of 3.3 m and an equivalent length of 2.9 m. The analysis was performed for 20-floor buildings. The use of these parameters for the analysis resulted in low coupling effects. The degree of coupling for a two-wall system is commonly determined as $\frac{T}{M_o}$ (Paulay, 2002), where T corresponds to the additional axial force generated by coupling (tension on one of the walls and compression on the other), l is the distance between the centroids of forces T and M_o is the bending moment applied to the wall system. To generate cases with a high coupling level, slender walls with low amounts of boundary reinforcement were connected via strong coupling elements.

The reduced elastic response can be estimated based on the coupling level as suggested by Priestley *et al.* (2007). However, considering various configurations of coupled walls and a building design that is based on the implementation of computational models, an alternative method for estimating the coupling effect is suggested.

4.2. Elastic displacement model

Higher coupling in the system generates moment diagrams in which the signs for the upper floors of buildings change, as shown in Fig. 9(a). Note that longer walls are stiffer and stronger, which results in lower coupling levels, reduces the ratio between the minimum and maximum moments and moves the inflection point to the upper floors.

For slender walls, the elastic displacement can be calculated by integrating the distribution of curvature over the height. Based on this notion, a method for calculating the yield displacement from the curvature distribution of height for coupled walls is proposed. First, the yield curvature (ϕ_y) at the base of the wall and the yield roof displacement (δ_y) are determined, as previously described for uncoupled walls, using the axial load that exists at the base of the walls. This load can be directly obtained from the design building model that already incorporates coupling. A capacity design method can be used to estimate the axial load due to coupling (Priestley *et al.*, 2007).

The curvature distribution can be approximately calculated from the moment distribution, $M(h) = M_y(h_w - h_o)(h_w^3 h_o - h_w h_o^3)h^3 + M_y(h_o^3 - h_w^3)(h_w^3 h_o - h_w h_o^3)h + M_y$, as shown in Fig. 9(b), which is based on a cubic function with varying height (h) that is dependent on the yield moment, M_y ; the wall height, h_w ; and the height to the inflection point, h_o . The distribution of stiffness in height can be approximated by the value $EI_{cr} = \frac{M_y}{\phi_y}$ at the base, which increases linearly to a height h_x , where it becomes a constant value and is assumed to be the uncracked stiffness EI_g (Fig. 9(c)). To simplify the analysis, it is assumed that $h_x = h_o$ and $EI_{cr} = 0.4EI_g$. Based on these assumptions, the yield displacement for coupled walls is analytically estimated. Eq. (12) provides an approximation of the general solution that is dependent on the uncoupled (δ_y) yield displacement, the height of the wall and the inflection point. The latter can be estimated from the wall moment diagrams of the implemented building model.

$$\delta_{y_coupled} = \delta_y \left(1.4 \frac{h_o}{h_w} - 0.37 \right)^{0.4} \quad (12)$$

For the analysis, walls with low and high couplings (variation in wall and slab reinforcement) were considered for walls with lengths of 2.5 m, 3.5 m and 5 m. In Fig. 10, the estimation of the yield

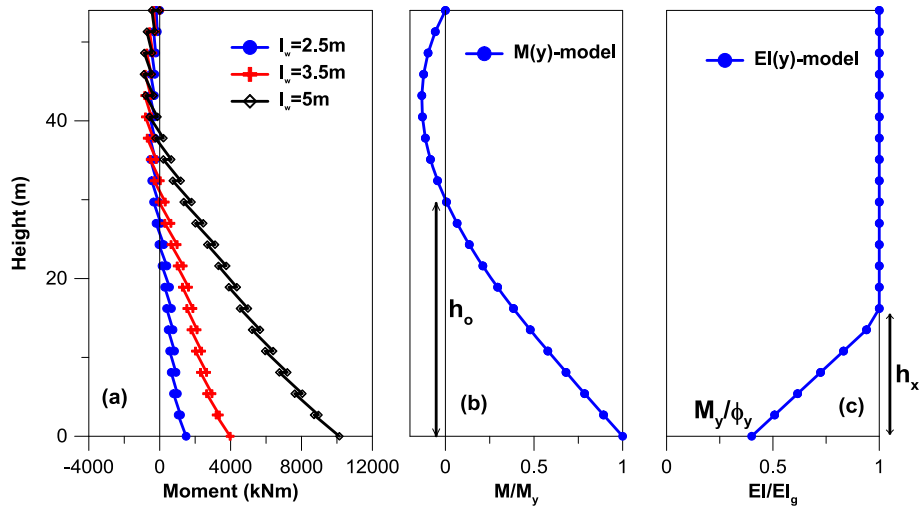


Figure 9. Coupled walls: (a) moment diagram for different wall lengths, (b) approximated moment distribution along the height, and (c) approximated stiffness distribution (flexure) along the height.

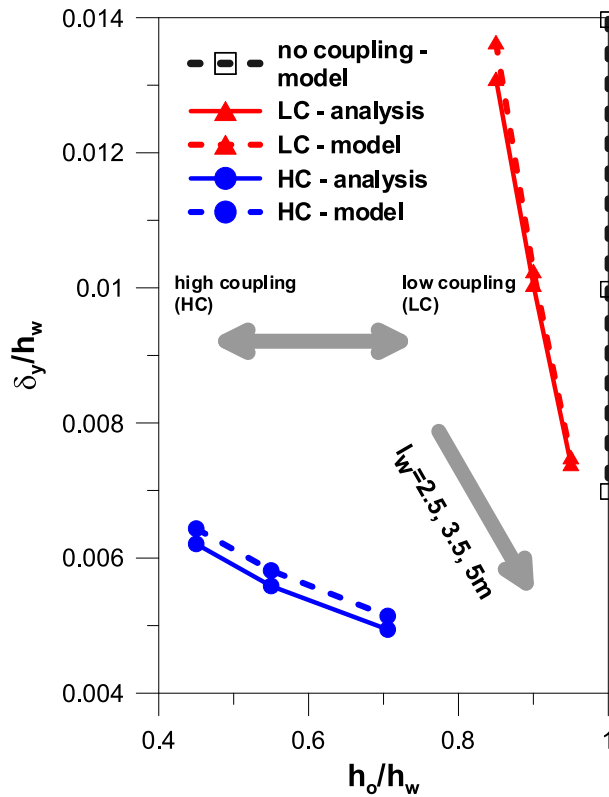


Figure 10. Yield displacement estimation for coupled walls.

displacement considering coupling is compared with the fiber model with coupling between two walls (analyses were performed for the wall with lower axial load due to coupling because it yields first). For the model estimation, the equations for the yield displacement for uncoupled walls are employed (Eqs. 2–5) with the axial load incorporating the coupling effect. The h_o value is estimated as the first zero value that crosses (from the base) the moment diagram in the fiber model. Walls with low and high levels of coupling exhibit satisfactory agreement between the predicted values using the proposed method and the values obtained from the numerical analysis. The model exhibits the same trend, which

increases or decreases the yield displacement for the different cases. Larger coupling produces lower values of h_o/h_w and a reduction in the yield displacement. Longer walls (l_w) exhibit a lower coupling effect and a lower uncoupled yield displacement.

5. INELASTIC DISPLACEMENT COMPONENT—PLASTIC HINGE MODEL

Eq. (1) can be used to estimate the curvature demands (or strains in the most compressed boundary wall) after the elastic limit is exceeded. Simplified expressions, such as Eq. (13), have been used to determine confinement requirements in design (e.g. ACI 318-08, 2008; Moehle, 1992; Wallace and Orakcal, 2002) based on a hinge at the base of the wall, where all curvature is represented by an equivalent rectangle (Fig. 2(b)). A hinge length of $0.5 l_w$ is a common assumption.

$$\phi_u = \frac{\delta_u}{h_w l_p} \quad (13)$$

The plastic hinge length for walls has been studied by several authors, including Paulay and Uzumeri (1975), who adapted an equation that was proposed for beams, as demonstrated by Eq. (14). Paulay and Priestley (1993) recommend $\alpha_1 = 0.5$ and $\beta_1 = 0.044$ for a lower limit in Eq. (14).

$$l_p = \alpha_1 0.8 l_w + \beta_1 h_w \quad (14)$$

Other expressions have incorporated effects such as shear, strain penetration (Hines *et al.*, 2004) or the level of axial load (Bohl and Adebar, 2011). Regarding shear or strain penetration, two considerations should be considered: first, the impact over the wall top displacement and second, its effect over the local strain within the plastic hinge. Shear in relatively slender walls (aspect ratio of 3 to 4) accounts for approximately 30% of the lateral displacement at the location of the plastic hinge; however, this value reduces to approximately 10% for the top displacement (Massone and Wallace, 2004). This result indicates that its effect on the top displacement can be neglected if a conservative analysis is required, but diagonal cracking locally impacts the strains at the plastic hinge. This effect is more important in shorter walls or walls with discontinuities. A detailed analysis is required, which is beyond the scope of this work. Strain penetration only impacts the top displacement. The experimental evidence in walls indicates that it may account for approximately 10% of the top displacement for walls with an aspect ratio of 2.3 (Dazio *et al.*, 2009) and therefore can be neglected in most cases. Regarding the axial load, Bohl and Adebar (2011) investigated the dependency of the plastic hinge length to the axial load from a finite element model, resulting in Eq. (15), which is limited to $0.8 l_w$. The analysis was primarily performed for roof drift levels of 2%. The expression indicates that high levels of axial load (e.g. $0.35 f'_c A_g$) may reduce the plastic hinge length by 50% compared with the case without axial load. In Eq. (15), the variable z recognizes that the plastic hinge length is impacted by the moment-shear ratio at the plastic hinge location, assumed at the wall base ($z = M/V$), which is related to the location of the resultant lateral force. The calibration of Eq. (15) was performed considering a point load applied at the wall top, where $z = h_w$. Recently, it has been recognized that the plastic hinge length typically increases with increasing drift levels (Kazaz, 2013).

$$l_p = (0.2 l_w + 0.05 z) \left(1 - \frac{1.5 P}{f'_c A_g} \right) \quad (15)$$

Other parameters that may impact the wall response include hardening of the reinforcement, the amount of boundary reinforcement and the inelastic roof drift level. To examine the impact of these

variables, a numerical nonlinear analysis of the implemented models is performed. For boundary elements properties, the confined concrete model by Saatcioglu and Razvi (1992), considering the amounts of transversal reinforcement required by the American Concrete Institute 318-08 (2008), is employed; confinement of 40% of the length of the wall on each side is provided to minimize early degradation problems.

A parametric analysis is performed, in which the following variables are varied: (1) the axial load values are $0.15f'_c A_g$, $0.2f'_c A_g$ and $0.3f'_c A_g$, which are typical values in Chilean construction (Estay, 2008); (2) the wall length values are 2.5 m, 5 m and 7.5 m; (3) three different heights that correspond to buildings with 10, 15 and 20 floors were considered; (4) the amount of boundary reinforcement values are 2.5%, 5% and 7.5% of the boundary area, since a common value for Chilean buildings is approximately 5% (Estay, 2008); (5) the hardening is defined as $b = E_p/E_s$ (ratio of post-yield to pre-yield steel stiffness), and the values selected are 2%, 3% and 4% with a strain at hardening initiation (ϵ_{sh}) of ϵ_y (0.0021—yield strain), 1% and 2%; and (6) different drift levels are analyzed. Generally, drift levels of 1%, 1.5%, 2% and drift values associated with compressive strains in concrete of 0.003 and 0.008 are considered.

Generally, the plastic hinge length $l_p = 0.5l_p^*$, where l_p^* is the distance from the wall base to the point at which the yield strain is attained in the reinforcing bar that is subjected to tension. Therefore, the equivalent rectangle for plastic curvatures is consistent with a linear distribution of plastic curvature over l_p^* . For consistency in this study, l_p^* is defined for the first yield, tracking yielding in the extreme tensile reinforcement along the height of the wall. From the results of the numerical analysis, a regression was performed to modify the expression proposed by Bohl and Adebar (2011), as shown in Equation (16). Eq. (16a) is calibrated for a variable z , which is used for additional analysis, whereas h_w was selected for Eq. (16b) to verify the correlation with the previous results. The analysis results indicate that the plastic hinge length increases with the level of plastic displacement or drift $\Delta_p = \frac{(\delta_u - \delta_y)}{h_w}$ instead of the total drift, starting from zero plastic hinge length at zero plastic drift, which is consistent with the inexistence of inelastic deformation. Because the amount of boundary reinforcement and hardening has less impact, they are not included in Equation (16).

$$l_p = (0.2l_w + 0.05z) \left(1 - \frac{1.5P}{f'_c A_g} \right) (6.7\Delta_p^{0.3}) \quad (16a)$$

$$l_p = (0.2l_w + 0.05h_w) \left(1 - \frac{1.5P}{f'_c A_g} \right) (5.1\Delta_p^{0.3}) \quad (16b)$$

Fig. 11 shows the values of the plastic hinge length estimated by Eq. (16a) compared with the values obtained from the numerical analysis (fiber model). The discrepancies are associated with the parameters that were not incorporated in the model. The figure includes the estimation of the plastic hinge for an imposed 0.8% plastic drift, which corresponds to the average value of plastic drift levels used in the analysis (total drift levels range between 0.6% and 3%, which yields plastic drift levels between 0.1% and 2%). The effect of drift significantly impacts the correct estimation of l_p , where the estimate for the fixed drift value reduces the plastic hinge length by approximately 30% in some cases and doubles the length compared with the calibrated expression with the consistent plastic drift (Eq. (16a)). Fixing the plastic drift to a certain level is intended to show the differences that could be expected compared with other plastic hinge length models (e.g. Bohl and Adebar, 2011) that do not include the impact of plastic drift level. Although small plastic drift levels recover the expression from Bohl and Adebar (and other expressions as well), some of the formulations for plastic hinge length from the literature have been calibrated in order to better predict the maximum curvature for design (usually detailing), and therefore, formulations would match as curvature comparison rather than plastic hinge length comparison. As explained in the next paragraphs, the distribution of curvature along the plastic hinge length is an important parameter that needs to be taken into account in order to correctly predict the maximum

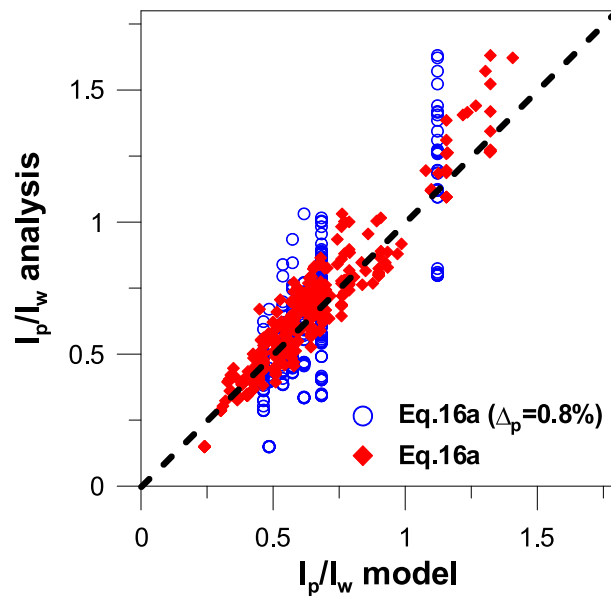


Figure 11. Plastic hinge length prediction versus analysis (fiber model).

curvature. The distribution of curvature is further incorporated as a factor (see β in Eq. (17)) that accompanies the plastic hinge length and therefore could be considered as a modification of its value.

A correct estimate of the plastic hinge length does not guarantee a correct estimate of the curvature demand. The behavior of steel is highly relevant in the curvature at the wall base and the distribution over height (Dazio *et al.*, 2009). Thus, the effect of the steel behavior on the distribution of curvature along the height is examined. In Fig. 12, the distribution of curvature over the height is shown for walls of buildings with 20 floors and a length of 5 m with different steel properties (variation in ρ_b , ε_{sh} and b) for a drift of 1.5%, which corresponds to a 0.7% plastic drift. Considering that the yield point ($l_p^* = 2l_p$) is at a height ranging from 6.5 to 7.7 m (20% change) for all cases, the maximum curvature values range from 0.0036/m to 0.0089/m (150% change), which indicates that the differences relate to how the curvature varies below the yield point rather than the plastic hinge length. Thus, a linear distribution assumption may not be adequate in all cases. This finding is consistent with the important curvature variation at the wall base, which was experimentally observed by Dazio *et al.* (2009), where the axial load, the reinforcement quantity and the steel hardening properties differed.

In order to capture the different curvature distribution observed in Fig. 12, a modified expression of Eq. (1) for the ultimate curvature is proposed (Eq. (17)). The new expression considers an inelastic nonlinear curvature distribution of the type $\phi(y) = (\phi_u - \phi_y) \left(\frac{y}{l_p}\right)^{(2/\beta-1)} + \phi_y$, where y is measured along the height of the wall from the yield point to the bottom and β is a parameter related to the way the curvature increases (in general, $\beta < 1$ and $\beta = 1.0$ for linear distribution). Thus, the plastic rotation is given by $\theta_p = \beta(\phi_u - \phi_y) \left(\frac{l_p}{2}\right) = \beta l_p (\phi_u - \phi_y)$. Considering that $h_w \gg \frac{l_p}{2}$ in tall buildings, the expression for the ultimate curvature reduces to

$$\phi_u = \phi_y + \frac{(\delta_u - \tilde{\delta}_y)}{\beta l_p (h_w - \frac{l_p}{2})} \quad (17)$$

Although factor β in Eq. (17) is considered to be a reduction of the plastic hinge length, it is related to the concentration of curvature toward the most critical zone within the plastic hinge length. This

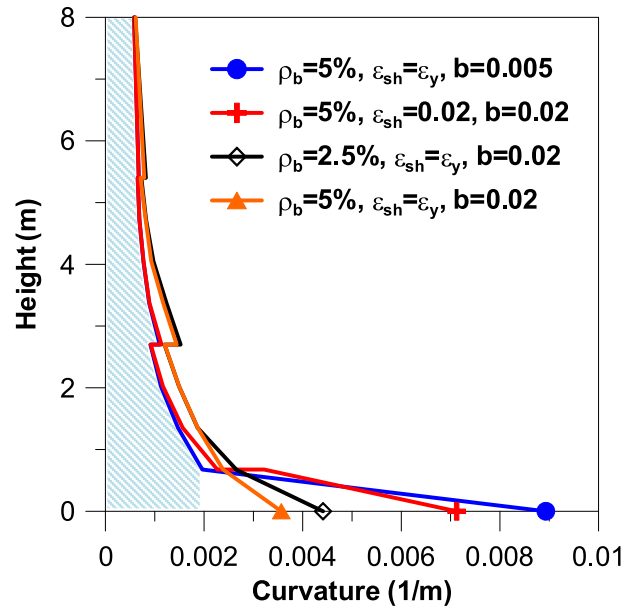


Figure 12. Curvature distribution along the height.

expression also includes a correction of the yield displacement component δ_y determined at first yield. Fig. 12 describes the curvature distribution along the height of the wall reaching a curvature beyond yielding at wall base. The location of the yield curvature ϕ_y defines the end of the plastic range. Double integration of the elastic curvature (shaded area for the curvature distribution with the largest maximum curvature) yields the elastic top displacement. Upon increment of lateral top displacement, yielding of the boundary reinforcement progresses, moving upwards along the height of the wall increasing the shaded area, and therefore increasing the elastic lateral top displacement for this formulation. Thus, the corrected yield component ($\tilde{\delta}_y$) is calibrated as $\tilde{\delta}_y = \delta_y \left[1 + 0.9 \left(\frac{l_p}{h_w} \right)^{0.23} \right]$.

Generally, $\tilde{\delta}_y \approx 1.4\delta_y$.

As it was shown in Fig. 12, given the location of the yield point, and therefore the length of the plastic zone within the wall height, inelastic distribution of curvature is mostly dependent on steel properties. Thus, parameter β is dependent on the onset of hardening (ε_{sh}) and the post-yield relative stiffness (b), as well as the boundary reinforcement ratio (ρ_b), assuming that the web-distributed reinforcement is less representative. As a simplified model, an expression consistent with an increase in post-yield force per unit area of the boundary element of the wall that corresponds to $E_s b \rho_b (\varepsilon_s - \varepsilon_{sh})$ is proposed, with ε_s tensile steel strain in the tension wall boundary. Considering that ε_s is associated with the top lateral displacement of the wall, for simplicity, the expression is only calibrated with material properties and steel quantity as shown in Eq. (18). The expression is valid for the range of parameters considered, which vary between ε_y (0.0021) and 0.02 for ε_{sh} , between 0.005 and 0.075 for ρ_b and between 0.005 and 0.04 for b . Note that for $b = 0.04$, $\rho_b = 0.075$ and $\varepsilon_{sh} = \varepsilon_y$, it practically recovers the original expression because $\beta = 0.87$. Other cases yield smaller values for β , which increases the curvature. Eqs. (17) and (18) together are capable of predicting the variation of curvature observed in Fig. 12.

$$\beta = 10(b\rho_b)^{0.42} \left(1 - (\varepsilon_{sh} - \varepsilon_y)^{0.22} \right) \quad (18)$$

The accuracy of the proposed expression is presented in Fig. 13. In Fig. 13, the ratio between the estimated curvature and the theoretical ultimate curvature is shown as a function of the parameters associated with coefficient β and the trend line. For the calculation of the ultimate curvature, the

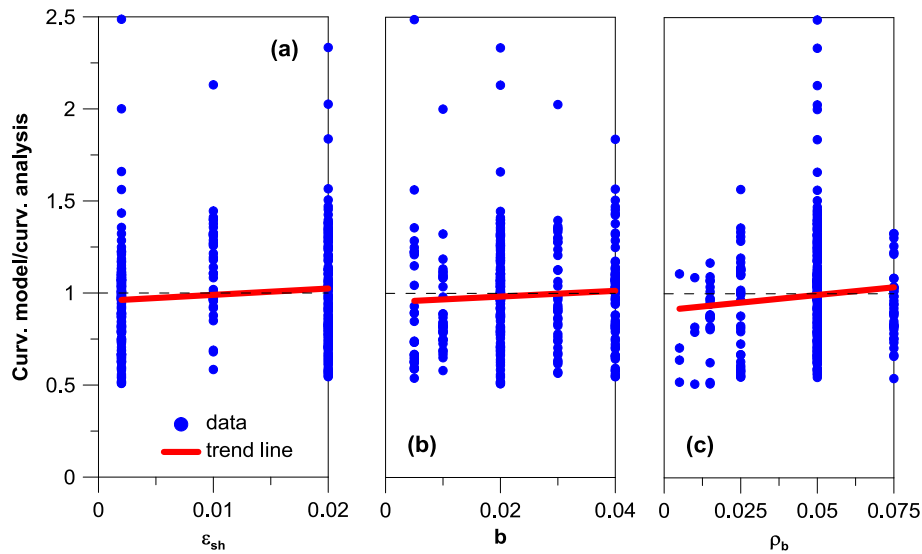


Figure 13. Ratio of curvature prediction of proposed model versus analysis (fiber model) to the β coefficient: (a) variation in ε_{sh} , (b) variation in b , and (c) variation in ρ_b .

following assumptions for the yield component are considered: $K = 1.4$, $\alpha = 0.22$ and $\tilde{\delta}_y \approx 1.4\delta_y$ because generally, the displacement demands significantly exceed the elastic response. As shown for each of the parameters (b , ρ_b and ε_{sh}), the curvature estimation is capable of capturing its effect (trend lines almost horizontal). Few cases (less than 3%) present a significant overestimation (above approximately 1.5), which is obtained in cases with low curvature values, where an error (simple model) in the yield estimate increases the predicted curvature.

In Fig. 14(a), the estimation of the curvature (Eq. (17)) versus the curvature obtained from the analysis (fiber model) is shown for the same cases examined for the plastic hinge length. Additionally, the ultimate curvature is also estimated from Eq. (13), which considers the plastic hinge length $l_p = l_w/2$ (Fig. 14(b)). The data are separated into two groups: the first group (solid symbols) covers roof displacements less than or equal to $1.5\% \frac{N}{20}$ with N number of floors and the second group (empty symbols) considers higher levels of lateral displacements. These levels of demand can be expected in rigid buildings with a large number of walls and soil conditions of moderate quality, which is common in many cases in building designs in Chile (Wallace *et al.*, 2012). In Fig. 14(a), the estimated average curvature values are similar to the values obtained from the numerical analysis with a mean value of 0.99 and a dispersion of 0.28. If we consider the cases with low drift demand (solid symbols), the plastic hinge length (Eq. (16a)) can be approximated by $l_p = 0.17l_w + 0.027h_w$, which yields a slightly higher mean value and dispersion for the group. Fig. 14(b) shows that Eq. (13) is more conservative in general (avg = 1.8) in estimating the ultimate curvature but has a large dispersion (sd = 1.35), which indicates that it is not conservative for an important number of cases.

Experimental validation of the proposed methodology is difficult because few experimental studies of slender walls have investigated precise curvature values at the wall base. Dazio *et al.* (2009) tested six relatively slender walls (aspect ratio = 2.3) with a point load under increasing lateral displacement cycles. The walls had different configurations of distributed and boundary longitudinal reinforcement, confinement and axial load. The properties of steel that were used for reinforcement also showed different hardening values, which are relevant information for this discussion. The main characteristics are described in Tab. 1, in which the level of axial load ($N/f_c A_g$), boundary reinforcement ratio (ρ_b) and distributed reinforcement ratio (ρ_w), as well as the yield stress (f_y) and maximum stress (f_m), are reported. The yield stress is estimated to the point of intersection in the stress versus strain curve with a line parallel to the elastic response beginning at 0.2% strain. The maximum stress is estimated at 2% strain, which is used for the relative post-yield stiffness (b) for distributed and boundary reinforcements. This test program helps in examining the effect of the coefficient β in the wall response because

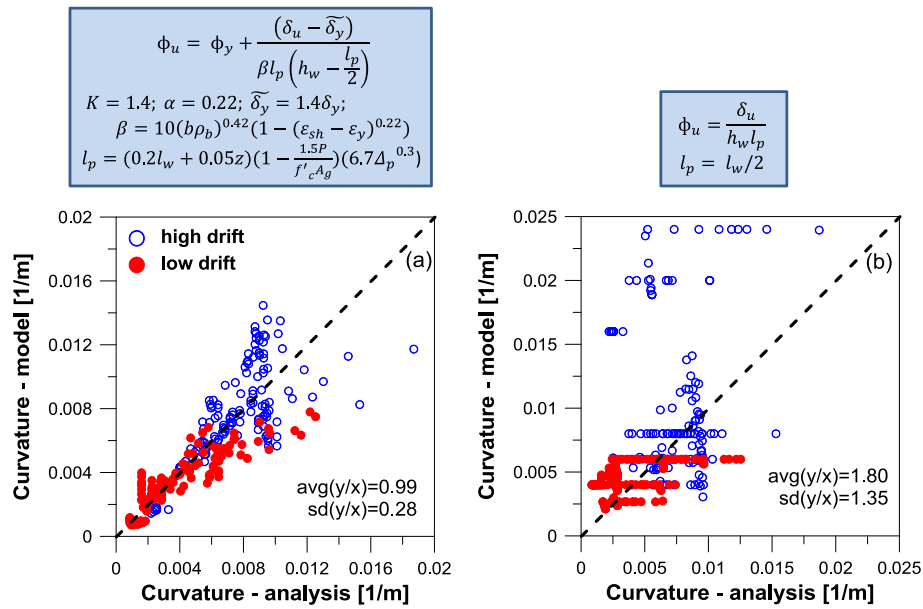


Figure 14. Curvature prediction versus analysis (fiber model): (a) proposed model and (b) simple plastic hinge.

Table 1. Wall test characteristics (Dazio *et al.*, 2009).

ID	$N/f'_c A_g$	ρ_b	ρ_w	ρ_{eq}	h_w	l_w	$f_{y,b}$	$f_{m,b}^2$	$f_{y,w}$	$f_{m,w}^2$	b_b	b_w	b_{eq}
-	-	%	%	%	m	m	MPa	MPa	MPa	MPa	-	-	-
WSH2	0.057	1.32	0.3	1.52	4.56	2.0	583	683	485	517	0.033	0.010	0.022
WSH3	0.058	1.54	0.54	2.37	4.56	2.0	601	676 ¹	569	648 ¹	0.025	0.026	0.025
WSH4	0.057	1.54	0.54	2.37	4.56	2.0	576	636	584	656	0.020	0.024	0.022
WSH5	0.128	0.67	0.27	0.73	4.56	2.0	584	656	519	543 ¹	0.024	0.008	0.015
WSH6	0.108	1.54	0.54	2.37	4.52	2.0	576	636	584	656	0.020	0.024	0.022

¹Estimated with similar overstrength as other specimens.

²Determined at 2% strain.

the reinforcement properties and amounts vary among the different walls. Fig. 15 shows the experimental results from Dazio *et al.* (2009) and the curvature estimation as a function of wall top drift. The simplified estimate of the yield component is considered. For all cases, the drift value is based on the flexural component, which accounts for 80% of the total roof displacement. According to the experimental results, approximately 20% of the displacement corresponds to shear and the deformation due to strain penetration (each with a similar contribution). Although the formulation was proposed assuming that the web reinforcement is not as important as the boundary longitudinal reinforcement, in cases with large amount of web reinforcement or low amounts of boundary reinforcement, an equivalent value for the amount of reinforcement and hardening was estimated, because the contribution of distributed reinforcement was important in some cases. The amount of reinforcement, boundary and web steel ratios were weighted by the area of concrete (to ensure that it is influential as a function of tensile force) and location with respect to the compressed boundary (to ensure that it is influential as a function of moment arm), in which a distributed amount of 0.25% (used in the model formulation) is discounted to deliver an equivalent force at the wall boundary. Thus, in walls with a distributed reinforcement larger than 0.25%, an equivalent reinforcement that is larger than the boundary reinforcement is produced. Similarly, the hardening (b) was estimated by weighting the force that contributes from the boundary and the distributed reinforcement. However, a distributed amount of 0.25% was not discounted because the value of the hardening applies to all distributed reinforcement. In all cases, $\varepsilon_{sh} = \varepsilon_y$. The estimation of equivalent parameters that combines boundary with web reinforcement

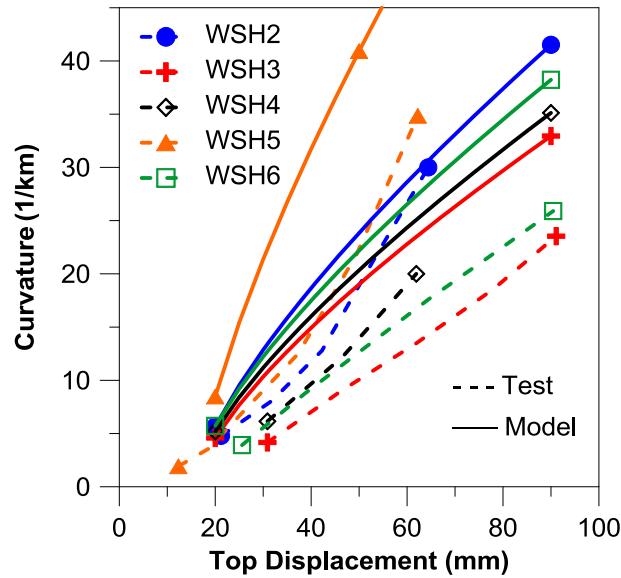


Figure 15. Curvature versus top displacement: test (Dazio *et al.*, 2009) and proposed model.

impairs a perfect comparison but gives a good guideline relative to the impact of the material characteristics. The results indicate that although the model overestimates the curvature values, there is a consistency regarding which cases exhibit larger curvature. WSH5 shows the largest curvature values, which are associated with a low amount of reinforcement, low hardening and are subjected to high axial loads. WSH2 shows the second highest curvature values that are primarily attributed to a small amount of reinforcement. Smaller curvature values are observed with WSH3; they are associated with a large amount of reinforcement and hardening values and a low axial load. This correlation is observed in the test and the model. WSH6 and WSH4 exhibit a different behavior between the model and test data. Higher experimental values of curvature are observed in the case of WSH4 compared with WSH6, which occurs in reverse in the model. The difference between these two cases is associated not only with the axial load level (considered in the model by the plastic hinge length) but also with the difference in confinement. Confinement consists of closed stirrups for WSH6 with an amount of approximately 0.4%, whereas WSH4 only considers U-shaped transversal reinforcement, which provides no real confinement or bar buckling restraint (Wallace *et al.*, 2012; Massone *et al.*, 2012). Specimen WSH4 will begin to degrade its capacity earlier due to the low ductility of the concrete at the boundary and lower capacity of boundary reinforcement, which results in a rapid increase in curvature values. The model assumes adequate confinement and bar buckling restraint; therefore, it is unable to capture this type of damage.

Although the correlation between the different walls is consistent with the model and the experimental data, the observed values differ. These differences might be associated with the way the curvature values were estimated in the test program. Considering that strains at the wall base and curvatures are affected by shear strain and strain penetration, Dazio *et al.* (2009) assumed a linear curvature distribution within the plastic hinge (used five or six points to estimate curvature values within l_p^*), excluding the last point (to prevent shear and strain penetration), and extrapolated the curvature to the wall base by using the aforementioned measurements. Although the specimens were well-instrumented, a different assumption than a linear curvature distribution is probably impractical. Thus, if the actual curvature distribution is nonlinear ($\beta < 1$), this procedure underestimates the curvature at the wall base. Estimates for assumptions with a nonlinear distribution ($\beta < 1$) used to derived Eq. (17) indicate that the experimental results for the curvature at the base might have been reduced by about 50% for $\beta = 0.4$ (average value for the specimens under analysis) by using a linear interpolation. More detailed instrumentation could help providing valuable experimental information. This result assumes the comparison of continuous curves, whereas the wall tests considered discrete values, which would reduce this effect.

All this explains the apparent overestimation of curvature estimates with the model at wall base, but the experimental data do not provide enough discretization that could reduce the uncertainty in the information required for this analysis.

6. CONCLUSIONS

This study presents a parametric analysis using a fiber nonlinear model of slender reinforced concrete walls, which facilitates calibrating expressions for yield curvature, yield displacement, plastic hinge length and distribution of curvature at the wall base.

A series of monotonic analyses of rectangular walls with a triangular lateral load distribution that considers different variables, such as axial load and the amount of boundary reinforcement, are performed. From these analyses, an expression that estimates the yield curvature (related to K) is determined based on axial load and boundary reinforcement. However, a conservative value of $K=1.4$ can be used. An analytical expression based on parameter α for estimating the yield displacement, which is dependent on the amount of boundary reinforcement, is calibrated. Based on the numerical analysis, $\alpha=0.22$ can be conservatively assumed. In the case of T-shaped walls, similar results to rectangular walls are obtained when the web is in compression. When the flange is in compression, the values $K=1.0$ and $\alpha=0.22$ are conservatively assumed.

The numerical model that incorporated coupling between walls by slab action resulted in low coupling for common Chilean design. A general procedure is proposed to account for coupling in the estimation of yield displacement, which is based on the estimation of the displacement of walls without coupling and the location of the inflection point in the moment diagram, whose value can be obtained from the design models. Adequate correlation between the prediction and the analysis was observed with this methodology for low and high levels of coupling.

The inelastic response is used to calibrate an expression for the plastic hinge length. A set of numerical analyses are conducted considering several variables, such as axial load, wall length and height and drift level. Incorporating the plastic drift (Δ_p) attained by the wall improves the estimation of the plastic hinge length. For example, the estimation of the plastic hinge for an imposed 0.8% plastic drift results in a reduction of the plastic hinge length by approximately 30% for some cases; in other cases, it doubles the length compared with the calibrated expression (Eq. (16a)).

Variations in properties of steel, such as hardening and the reinforcement ratio, indicate that the distributions of curvature below the yield point (along the wall height) are nonlinear, which requires a β factor to correct the traditional expression that helps to estimate the curvature demand. It is partially validated with experimental data from the literature, which indicates that the amount of reinforcement and hardening affect the ultimate curvature, as predicted by the proposed model. In the case where the plastic hinge length is estimated using $l_p=0.5l_w$ and the hinge model concentrate all curvature at the wall base, results are conservative with an important dispersion of results, which underestimates the curvature in many cases.

ACKNOWLEDGEMENTS

This study was financially supported by InnovaChile-Corfo under Grant No. 10CREC-8580 – “New Methodology for Seismic Design of Shear Wall buildings for the New Design Code” and partially supported by Chile’s National Commission on Scientific and Technological Research (CONICYT) for the project Fondecyt 2013, Regular Research Funding Competition under Grant No. 1130219. The contribution by ICH (Chilean Concrete and Cement Institute) CEO Augusto Holmberg is also acknowledged.

REFERENCES

- ACI 318-08. 2008. Building Code Requirements for Structural Concrete and Commentary. Committee 318. American Concrete Institute, Farmington Hills, Michigan.
- Alfaro J. 2013. Elastic and inelastic displacement estimates of slender walls for a plastic hinge model based on fiber modeling (in Spanish). Engineering thesis. Civil Engineering Department, University of Chile.
- Belarbi H, Hsu TCC. 1994. Constitutive laws of concrete in tension and reinforcing bars stiffened by concrete. *ACI Structural Journal* **91**(4): 465–474.

- Bohl A, Adebar P. 2011. Plastic hinge lengths in high-rise concrete shear walls. *ACI Structural Journal* **108**(2): 148–157.
- Dazio A, Beyer K, Bachmann H. 2009. Quasi-static cyclic tests and plastic hinge analysis of RC structural walls. *Engineering Structures* **31**(7): 1556–1571.
- Eslami A, Ronagh HR. 2014. Effect of elaborate plastic hinge definition on the pushover analysis of reinforced concrete buildings. *Structural Design of Tall and Special Buildings* **23**(4): 254–271.
- Estay C. 2008. Characteristics of reinforced concrete wall design in Chile (in Spanish). Civil Engineering Thesis. School of Engineering. University of Chile.
- Hines EM, Restrepo JI, Seible F. 2004. Force-displacement characterization of well-confined bridge piers. *ACI Structural Journal* **101**(4): 537–548.
- Kang S-M, Kim J-Y. 2014. Evaluation of deformation capacity including yield deformation in displacement-based design of special RC shear wall. *Structural Design of Tall and Special Buildings* **23**(3): 181–209.
- Kazaz I. 2013. Analytical study on plastic hinge length of structural walls. *Journal of Structural Engineering* **139**(11): 1938–1950.
- Massone LM, Bonelli P, Lagos R, Lüders C, Moehle J, Wallace JW. 2012. Seismic design and construction practices for RC structural wall buildings. *Earthquake Spectra* **28**(S1): S245–S256.
- Massone LM, Wallace JW. 2004. Load-deformation responses of slender reinforced concrete walls. *ACI Structural Journal* **101**(1): 103–113.
- Massone LM. 2013. Fundamental principles of the reinforced concrete design code changes in Chile following the Mw8.8 earthquake in 2010. *Engineering Structures* **56**: 1335–1345.
- Moehle JP. 1992. Displacement-based design of RC structures subjected to earthquakes. *Earthquake Spectra* **8**(3): 403–428.
- OpenSees. 2000. <http://opensees.berkeley.edu/>.
- Paulay T, Priestley MJN. 1993. Stability of ductile structural walls. *ACI Structural Journal* **90**(4): 385–392.
- Paulay T, Uzumeri SM. 1975. A critical review of the seismic design provisions for ductile shear walls of the Canadian Code. *Canadian Journal of Civil Engineering* **2**: 592–601.
- Paulay T. 2001. Seismic response of structural walls: recent developments. *Canadian Journal of Civil Engineering* **28**(6): 922–937.
- Paulay T. 2002. The displacement capacity of reinforced concrete coupled walls. *Engineering Structures* **24**(9): 1165–1175.
- Popovics S. 1973. A numerical approach to the complete stress–strain curve of concrete. *Cement and Concrete Research* **3**(4): 583–679.
- Priestley MJN, Calvi GM, Kowalsky MJ. 2007. Displacement Based Seismic Design of Structures. IUSS PRESS: Italy.
- Saatcioglu M, Razvi S. 1992. Strength and ductility of confined concrete. *Journal of Structural Engineering* **118**(6): 1590–1607.
- Spacone E, Filippou FC, Taucer FF. 1996. Fibre beam-column model for non-linear analysis of R/C frames I. Formulation. *Earthquake Engineering & Structural Dynamics*. **25**(7): 711–725.
- Wallace JW, Massone LM, Bonelli P, Dragovich J, Lagos R, Lüders C, Moehle J. 2012. Damage and implications for seismic design of RC structural wall buildings. *Earthquake Spectra* **28**(S1): S281–S299.
- Wallace JW, Orakcal K. 2002. ACI 318-99 provisions for seismic design of structural walls. *ACI Structural Journal* **99**(4): 499–508.

AUTHORS' BIOGRAPHIES

Leonardo M. Massone is an Associate Professor at the University of Chile in the Civil Engineering Department. He received his BS degree (1999) from the University of Chile, and his MS (2003) and PhD (2006) degrees from the University of California, Los Angeles. He teaches concrete design, advance concrete design and nonlinear analysis of structures classes. His research interests include analytical and experimental studies of reinforced concrete systems, with emphasis on seismic response.

Jorge I. Alfaro is a civil engineer at Rene Lagos Engineers and graduated from University of Chile in 2013.